Research Article

pISSN 2799-8525 · eISSN 2799-8681
J Powder Mater 2024;31(3):236-242

Journal of Powder Materials

Investigation of the Thermal-to-Electrical Properties of Transition Metal-Sb Alloys Synthesized for Thermoelectric Applications

Jong Min Park[1,2], Seungki Jo[1], Sooho Jung[1], Jinhee Bae[1], Linh Ba Vu[1,2], Kwi-Il Park[2], Kyung Tae Kim[1,*]

[1]Department of 3D Printing Materials, Korea Institute of Materials Science, Changwon, Gyeongnam 51508, Republic of Korea
[2]Department of Materials Science and Metallurgical Engineering, Kyungpook National University, Daegu 41566, Republic of Korea

The development of thermoelectric (TE) materials to replace Bi_2Te_3 alloys is emerging as a hot issue with the potential for wider practical applications. In particular, layered Zintl-phase materials, which can appropriately control carrier and phonon transport behaviors, are being considered as promising candidates. However, limited data have been reported on the thermoelectric properties of metal-Sb materials that can be transformed into layered materials through the insertion of cations. In this study, we synthesized FeSb and MnSb, which are used as base materials for advanced thermoelectric materials. They were confirmed as single-phase materials by analyzing X-ray diffraction patterns. Based on electrical conductivity, the Seebeck coefficient, and thermal conductivity of both materials characterized as a function of temperature, the zT values of MnSb and FeSb were calculated to be 0.00119 and 0.00026, respectively. These properties provide a fundamental data for developing layered Zintl-phase materials with alkali/alkaline earth metal insertions.

Keywords: Thermoelectric materials; Transition metal; Antimony; Electrical properties; Thermal conductivity

Received: March 26, 2024
Revised: April 24, 2024
Accepted: April 24, 2024

***Corresponding author:**
Kyung Tae Kim
Tel: +82-55-280-3506
Fax: +82-55-280-3474
E-mail: ktkim@kims.re.kr

1. Introduction

Thermoelectric (TE) technology is attracting attention for energy production and efficient energy utilization. In particular, compared to other renewable energy sources, it is the unique technology that can directly convert thermal energy into electric energy or provide heating and cooling through electricity without any driving part. Bismuth telluride (Bi_2Te_3)-based alloys have been considered as representative materials for practical TE applications [1-3]. That is due to suitable combination between low thermal conductivity caused by their layered structure composed of Van der Waals bonds and a good power factor ($S^2\sigma$, PF) resulting from the mixture of covalent and ionic bonds in the temperature range of 273 – 500 K. These characteristics result in a superior dimensionless thermoelectric figure of merit (zT), calculated by the formula $zT = (S^2\sigma T)/\kappa$ (S: Seebeck coefficient, σ: electrical conductivity, κ: thermal conductivity, and T: absolute temperature), in the room temperature region compared to other materials [4-6]. However, Bi_2Te_3-based materials are often limited in more wide applications due to their performance degradation outside the room temperature range and the scarcity and toxicity of raw materials. Therefore, various materials are being investigated as possible replacements for Bi_2Te_3 alloy.

Among these studies, zintl phase materials such as Yb-Mg-Sb and Na-Ga-Sn, which combine metals and nonmetals, are attracting attention for their excellent charge transfer and controllable thermal conduction [7-10]. Recently, zintl phase materials composed of alkali/alkaline earth metal-transition metal-pnictogen elements in atomic ratios of 1-1-1 and 1-2-2 are known to exhibit a layered structure similar to Bi_2Te_3, which is expected to result in thermoelectric performances [11-13]. Transition metals can easily accept electrons released by the ionization of alkali/alkaline earth metals due to their various oxidation numbers. In particular, transition metal-pnictogen materials composed of d_5 and d_{10} ions such as Zn^{2+}, Fe^{3+}, and Mn^{2+} have been reported to form layered structures with the

https://doi.org/10.4150/jpm.2024.00031

insertion of alkali/alkaline earth metals. [14, 15]. In addition, the energy bandgap of the material generally tends to decrease as the atomic radius of the pnictogen element(As, Sb, and Bi) in periodic table increases [16, 17]. Therefore, antimony (Sb) rather than bismuth (Bi) can be typically utilized to achieve the energy bandgap size of about a few hundred meV such as SnSe, Bi_2Se_3, and Bi_2Te_3. Toberer et al. synthesized AZn_2Sb_2 (A = Sr, Ca, Yb, Eu) through vacuum tube encapsulation followed by 15 hours of melting at 1223 K [18]. Based on their thermoelectric properties, the zT values of AZn_2Sb_2 (A = Sr, Ca, Yb, Eu) were calculated, resulting in maximum values of 0.35, 0.55, 0.4, and 0.9, respectively. Lian Wu et al. synthesized a material composed of $Mg_{3.2}Sb_2$ and $CaZn_2Sb_2$ mixed in a specific ratio using a ball mill process [19]. Based on thermoelectric characterization results depending on the ratio of $Mg_{3.2}Sb_2$ to $CaZn_2Sb_2$, the material with a 1:1 composition exhibited the maximum zT of 0.68 at 773 K. Although many recent studies have reported the evaluation of properties of layered zintl phases with inserted alkali/alkaline earth metals, most of them are synthesized based on ZnSb. As mentioned above, the d_5 and d_{10} transition metals such as Fe and Mn are also expected to exhibit thermoelectric properties, but there are no relevant studies so far despite high potential as TE materials.

In this study, we synthesized FeSb and MnSb-based alloys that can be used for the base materials of advanced TE materials showing layered-zintl-phase. The synthesized FeSb and MnSb ingots were powdered, and subsequently, single-phase materials were successfully identified through XRD analysis. The confirmed single-phase FeSb and MnSb ingots were then polished to size for characterization. The Seebeck coefficient, electrical conductivity, and thermal conductivity of FeSb and MnSb were measured to calculate zT as a function of temperature. The FeSb and MnSb fabricated by arc melting yielded maximum zT values of 0.00026 and 0.00119 at 473 K, respectively. We have successfully investigated TE properties of metal-Sb materials for cation insertion, although these values are somewhat low.

2. Experimental

2.1.Fabrication of Fe-Sb and Mn-Sb Materials

A vacuum arc furnace (VAF) process was used to synthesize transition metal-Sb ingot materials of FeSb and MnSb. The raw materials used were Fe (0.1-1.7 mm, 3N, Kojundo Chemical Laboratory CO., LTD), Mn (2-5 mm, 3N, Kojundo Chemical Laboratory CO., LTD.), and Sb (2-6 mm, 5N, TASCO) shots. Referring to the phase diagrams of Fe-Sb and Mn-Sb [20, 21], the raw materials were weighed in compositions of 56:44 and 52:48 at%, respectively. These weighed raw materials were then placed in the arc melting machine and subjected to 120 V voltage for 5 repeated melting cycles.

2.2. Characterization

The as-synthesized ingots were ground using an induction milling machine and then powdered by filtering the grounds with a 50 μm standard sieve. The as-prepared ingots and powders were analyzed for microstructure and crystalline phase using scanning electron microscopy (SEM, SU-6600, HITACHI) and X-ray diffraction (D/MAX-2500VL/PC, Rigaku). The both ingots were machined to specification by a polishing process for the measurement of electrical conductivity (σ), Seebeck coefficient (S), and thermal diffusivity (D). Thermoelectric properties were measured by using Netzsch's SBA458 Nemesis equipment and laser flash analysis (LFA467 HyperFlash, Netzsch) instruments, respectively, at temperatures ranging from 298 K to 473 K. To calculate thermal conductivity, the density (ρ) of the material was measured by the Archimedes method, and the heat capacity (C_P) was calculated using the Dulong-Petit law ($C_P = 3R/M$) [22-24]. Thermal conductivity (κ) was then calculated using the equation $\kappa = D_\rho C_P$. Additionally, Hall analysis (HMS-5500, ECOPIA) at 298 K was performed to evaluate the carrier concentration (n) and mobility (μ) to analyze the changes in the electrical properties of the ingots.

3. Results and Discussion

Fig. 1(a) illustrates a schematic diagram of the fabrication process of transition metal-Sb materials using the arc melting process, along with actual photographs of the synthesized MnSb and FeSb ingots. The coin-shaped ingots, approximately 20 mm in diameter, were successfully produced by irradiating the raw materials with a high-energy arc, leading to rapid melting, followed by rapid cooling facilitated by a cold Cu plate with flowing coolant. Figs. 1(b) and 1(d) depict the surface microstructure of the samples observed after polishing the MnSb and FeSb ingots, respectively. Both materials underwent repeated rapid melting and cooling, resulting in various internal defects such as pores and cracks. Nevertheless, the EDS mapping results demonstrated that each element such as Fe, Mn, and Sb is uniformly distributed overall. Figs. 1(c) and 1(e) display the XRD patterns of the synthesized powders of MnSb and FeSb,

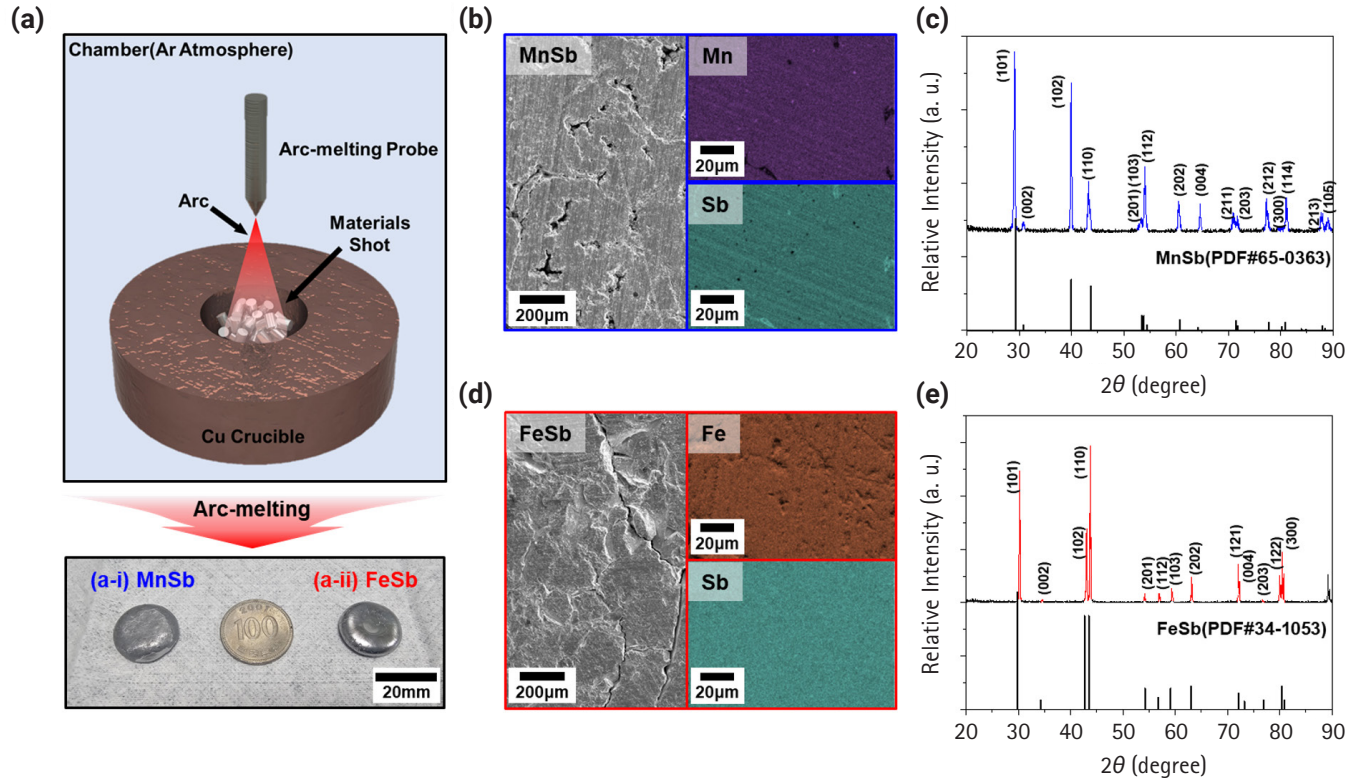

Fig. 1. (a) Schematic illustration of the arc-melting process and a photograph of synthesized MnSb and FeSb ingots. (b, c) Surface scanning electron microscopy (SEM), energy-dispersive spectroscopy (EDS) mapping image, and X-ray diffraction (XRD) patterns of synthesized MnSb. (d, e) Surface SEM, EDS mapping image and XRD patterns of synthesized FeSb.

respectively. According to the phase diagram mentioned in the experimental section [20, 21], the synthesis of single-phase FeSb and MnSb cannot be achieved smoothly when the ratio of Fe/Mn:Sb is 1:1. Materials synthesized with Fe-Sb and Mn-Sb compositions of 56:44 and 52:48 at% reveal good single-phase synthesis compared to the reference PDF card. This result suggests that we have successfully performed the first step for synthesizing a layered zintl phase.

Fig. 2 shows the results of the electrical properties of the ingots as a function of temperature ranging from 298K to 473K. Fig. 2(a) shows the variation of electrical conductivity with temperature for both synthesized FeSb and MnSb. The electrical conductivity of MnSb decreased from 3085 Scm^{-1} to 2145 Scm^{-1} with increasing temperature, exhibiting behavior typical of metals. This result is attributed to the metallic band structure of the majority spin electrons, although MnSb is a semiconductor [25]. Conversely, the electrical conductivity of FeSb increased from 330 Scm^{-1} to 414 Scm^{-1} with increasing temperature, exhibiting behavior typical of semiconductors. This result matches well with studies that FeSb is a semiconductor with a band gap [26]. Fig. 2(b) shows the Seebeck coefficient for both materials, showing a similar trend with negative values, confirming their N-type materials. Moreover, the mobility and carrier concentration of each material at room temperature were evaluated by Hall measurements (Fig. 2(c)). The mobility and carrier concentration of FeSb are 11.4 $cm^2V^{-1}s^{-1}$ and 2.88×10^{20} cm^{-3}, respectively, while those of MnSb are 151 $cm^2V^{-1}s^{-1}$ and 7.31×10^{20} cm^{-3}, respectively. The mobility of MnSb is about 10 times higher than that of FeSb, consistent with the substantial difference in electrical conductivity between the two materials observed in Fig. 2(a). Thus, it is feasibly confirmed that high electrical conducting behaviors of MnSb is due to high carrier concentrations and remarkably increased mobility compared to those of FeSb. Fig. 2(d) shows the calculated power factors based on the measured values of electrical conductivity and Seebeck coefficient, yielding 6.24 and 1.34 $\mu Wm^{-1}K^{-2}$ for MnSb and FeSb at 473 K, respectively.

Fig. 3 shows the comparison of the thermal conductivity of both alloys as a function of temperature. The density measured by the Archimedes method and the C_p value calculated by the Du-

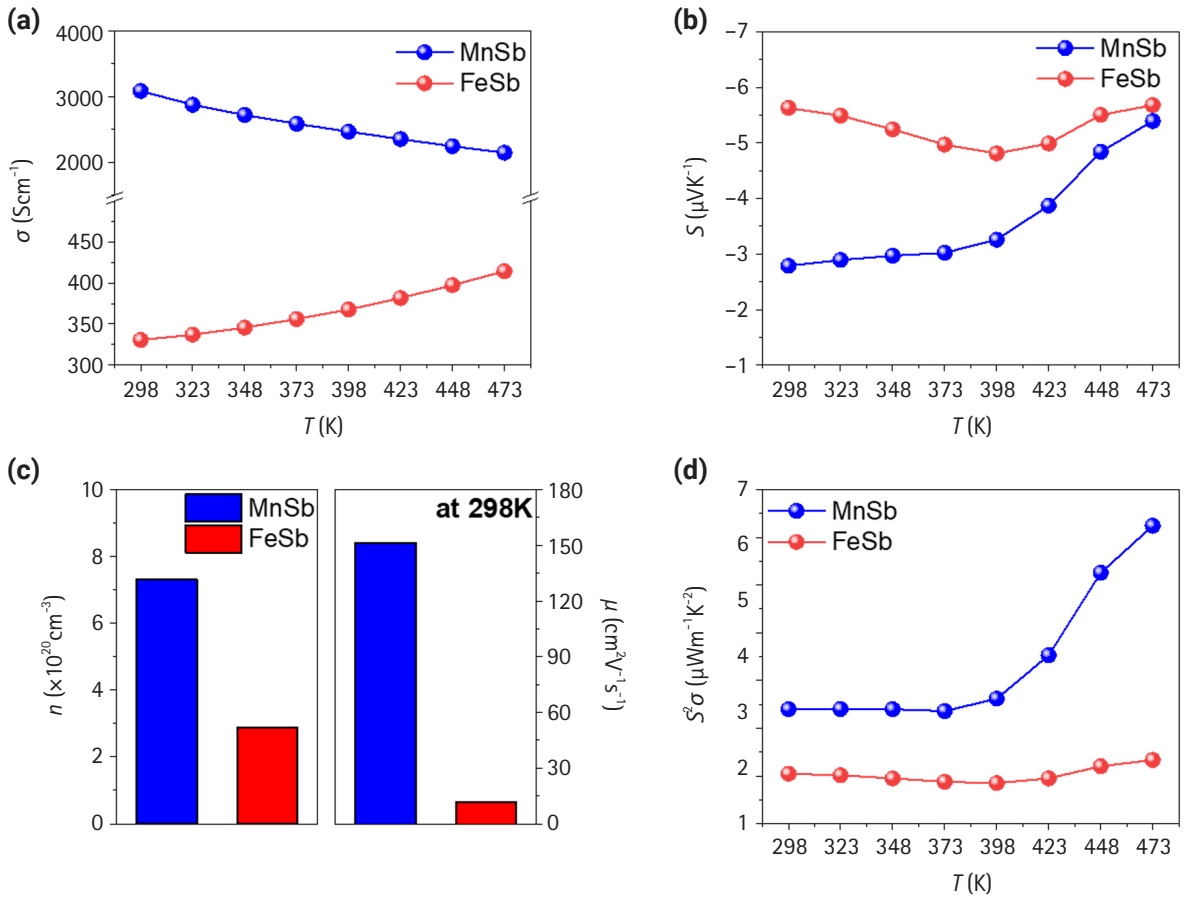

Fig. 2. Thermoelectric properties of MnSb and FeSb: (a) electrical conductivity, (b) the Seebeck coefficient, (c) carrier concentration and mobility, and (d) the power factor.

long-Petit law are presented in Table 1. The maximum thermal conductivity of MnSb was evaluated 2.74 $Wm^{-1}K^{-1}$ at 298 K, while the thermal conductivity of FeSb was evaluated 2.4 $Wm^{-1}K^{-1}$ at 473 K(Fig. 3(a)). These results are consistent with the behavior of the electrical conductivity depicted in Fig. 2(a).

Figs. 3(b) and 3(c) show the contribution of carrier ($\kappa_{e,cal}$) in total thermal conductivity and lattice thermal conductivity ($\kappa_{lat,cal}$) calculated using the following equations.

$$\kappa_{e,\,cal} = L\sigma T$$

$$L = 1.5 + \exp\left(-\frac{|S|}{116}\right)$$

$$\kappa_{tot} = \kappa_{lat,\,cal} + \kappa_{e,\,cal}$$

L is the Lorentz constant, which has units of 10^{-8} $W\Omega K^{-2}$ and was derived based on a computational approximation based on the single parabolic band model [27]. For both materials, a trend of increasing electronic thermal conductivity with rising temperature was observed. In the case of MnSb, the electronic thermal conductivity was calculated to reach up to 2.45 $Wm^{-1}K^{-1}$ as the temperature increased, which closely matched the measured total thermal conductivity at 473 K (2.47 $Wm^{-1}K^{-1}$). The lattice thermal conductivity of MnSb approached almost zero at 473 K, indicating that heat transfer inside the material strongly relies on electrons. That is, in spite of high electrical conductivity, it is analyzed that extremely low lattice thermal conductivity leads to decreasing-tendency of total thermal conductivity of the MnSb. Conversely, the calculated electronic thermal conductivity of the FeSb ingot reached up to 0.48 $Wm^{-1}K^{-1}$ at 473 K, constituting 20% of the total thermal conductivity evaluated in Fig. 3(a). This suggests that heat transfer in FeSb is highly dependent on the carrier rather than lattice phonon-scattering because lattice thermal conductivity shows similar values with increasing temperature. The analysis revealed differences in the primary heat transfer mechanisms with increasing temperature between FeSb and MnSb. MnSb exhibited

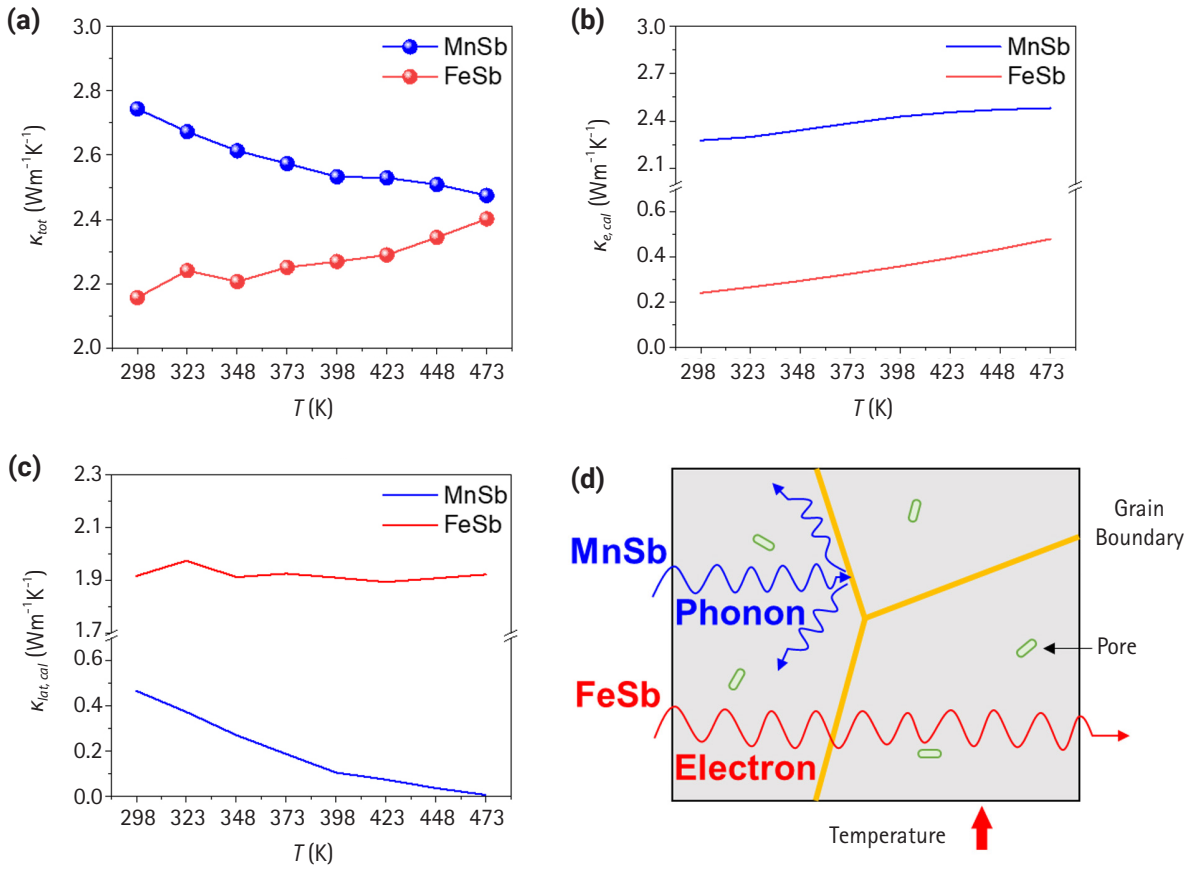

Fig. 3. (a) Total, (b) electronic, (c) and lattice thermal conductivity. (d) Schematic of the main mechanism for thermal conductivity of MnSb and FeSb.

Table 1. A comparison of measured density, calculated theoretical density [28,29], and calculated CP between MnSb and FeSb

Sample	Density (g·cm^{-3})	Theoretical Density (g·cm^{-3})	$C_{P,cal}$ (J·g^{-1}·K^{-1})
MnSb	6.342	6.79	0.141
FeSb	8.059	8.42	0.140

increased phonon scattering with increasing temperature, leading to a reduction in lattice thermal conductivity and an overall decrease in thermal conductivity. On the other hand, FeSb exhibited minimal change in lattice thermal conductivity, but an increase in electronic thermal conductivity due to enhanced carrier mobility, resulting in an overall increase in thermal conductivity (Fig. 3(d)).

Based on the evaluated electrical conductivity, Seebeck coefficient, and thermal conductivity as shown in Figs. 2 and 3, a dimensionless thermoelectric performances (zT) were calculated (Fig. 4). MnSb exhibited higher zT values compared to FeSb in all temperature range, with maximum zT values of 0.00119 and 0.00026 at 473 K, respectively. The maximum zT of MnSb was approximately 4.5 times higher than that of FeSb. Considering our aim in this study to achieve thermoelectric behaviors of two transition metal-Sb alloys as a function of temperature, TE properties of base materials was successfully obtained.

4. Conclusion

In this study, FeSb and MnSb, transition metal-pnictogen materials were synthesized and their fundamental thermoelectric properties were characterized for developing advanced TE materials through cation-insertion in base materials. The XRD patterns of the powderized FeSb and MnSb shows successful synthesis of single-phase materials. Subsequently, thermoelectric property evaluation of the machined single-phase FeSb and MnSb ingots produced zT values of up to 0.00026 and 0.00119

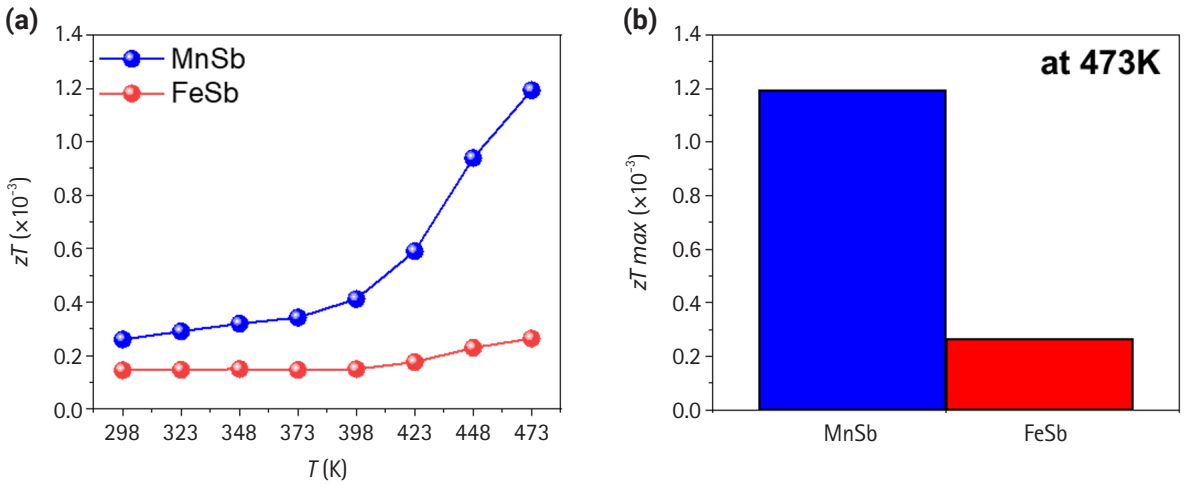

Fig. 4. (a) Temperature-dependent dimensionless figure of merit *zT* and (b) maximum *zT* of MnSb and FeSb.

at 473 K, respectively. The higher mobility observed in MnSb compared to FeSb aligns well with the results indicating high electrical conductivity at 298 K. Despite the relatively low zT values, this investigation into the thermoelectric properties of transition metal-pnictogen materials provides basic information for future advancements in layered zintl phase materials with alkali/alkaline earth metal insertions.

Conflict of Interest Declaration

S. Jo, K. -I. Park, and K. T. Kim serves as an editor of the Journal of Powder Materials editing, but has no role in the decision to publish this article. Except for that, no potential conflict of interest relevant to this article was reported.

Author Information and Contribution

J. M. Park : Ph.D. candidate, Conceptualization, Methodology, Investigation, Data curation, Formal analysis, Visualization, Writing – original draft, S. Jo : Senior researcher, Methodology, Validation, S. Jung : Senior researcher, : Resources, Validation, J. Bae : Senior researcher, Resources, Validation, L. B. Vu : M. S. Candidate, Resources, Validation, K. -I. Park : Professor, Conceptualization, Writing – review & editing, Supervision, Resources, K. T. Kim : Principal researcher, Conceptualization, Writing – review & editing, Supervision, Resources, Funding acquisition, Project administration.

Acknowledgments

This work was supported by the principal R&D program of Korea Institute of Materials Science (Code No. PNK9950) and Bridge-Convergence Technology R&D project (Code No. 2021M3C1C309754021) funded by National Research Foundation of Korea, respectively.

References

[1] S. Jung, Y. J. Woo, K. T. Kim, and S. Jo: J. Powder Mater., **30** (2023) 123.
[2] M. J. Jung, J. Y. Park, S. M. Eun, and B. J .Choi: J. Powder Mater., **30** (2023) 130.
[3] D. Bao, J. Chen, Y. Yu, W. Liu, L. Huang, G. Han, J. Tang, D. Zhou, L. Yang, and Z. Chen: Chem. Eng. J., **388** (2020) 124295.
[4] M. Rull-Bravo, A. Moure, J. F. Fernandez, and M. Martin-Gonzalez: RSC Adv., **5** (2015) 41653.
[5] T.M. Tritt and M.A. Subramanian: MRS Bull., **31** (2011) 188.
[6] A. J. Minnich, M. S. Dresselhaus, Z. F. Ren, and G. Chen: Energy Environ. Sci., **2** (2009) 466.
[7] S. Ohno, A. Zevalkink, Y. Takagiwa, S. K. Bux, and G. J. Snyder: J. Mater. Chem. A., **2** (2014) 7478.
[8] H. Tamaki, H. K. Sato, and T. Kanno: Adv. Mater., **28** (2016) 10182.
[9] T. Yamada, H. Yamane, and H. Nagai: Adv. Mater., **27** (2015) 4708.

[10] L. Borgsmiller, Q. Li, M. Y. Toriyama, and G. J. Snyder: Adv. Energy Mater., **13** (2023) 2300393.
[11] X. Zhang, H. Gu, Y. Zhang, L. Guo, J. Yang, S. Luo, X. Lu, K. Chen, H. Chai, G. Wang, X. Zhang, and X. Zhou: Chem. Eng. J., **374** (2019) 589.
[12] W. Zhang, C. Chen, H. Yao, W. Xue, S. Li, F. Bai, Y. Huang, X. Li, X. Lin, F. Cao, J. Sui, S. Wang, B. Yu, Y. Wang, X. Liu, and Q. Zhang: Chem. Mater., **32** (2022) 6983.
[13] S. Zheng, K. Peng, S. Xiao, Z. Zhou, X. Lu, G. Han, B. Zhang, G. Wang, and X. Zhou: J. Adv. Ceram., **11** (2022) 1604.
[14] J. Song, H. Y. Song, Z. Wang, S. Lee, J. Hwang, S. Y. Lee, J. Lee, D. Kim, K. H. Lee, Y. Kim, S. H. Oh, and S. W. Kim: Sci. Adv., **5** (2019) eaax039.
[15] C. Zheng: J. Solid State Chem., **72** (1988) 58.
[16] B. I. Yoo, N. Lee, B. Lamichhane, J. Bang, H. Y. Song, B. C. Park, K. H. Lee, S. Kim, and S. W. Kim: Adv. Mater., **34** (2022) 2200074.
[17] S. Khan, D. F. Khan, R. Neffati, T. Usman, M. W. Ahsraf, S. Khan, S. U. Jan, and G. Murtaza: J. Rare Earths., **42** (2024) 147.
[18] E. S. Toberer, A. F. May, B. C. Melot, E. Flage-Larsen, and G. J. Snyder: Dalton Trans., **39** (2010) 1046.
[19] L. Wu, Z. Zhou, G. Han, B. Zhang, J. Yu, H. Wang, Y. Chen, X. Lu, G. Wang, and X. Zhou: Chem. Eng. J., **475** (2023) 145988.
[20] D. Boa, S. Hassam, G. Kra, K. P. Kotchi, and J. Rogez: Calphad., **32** (2008) 227.
[21] P. Kainzbauer, K. W. Richter, and H. Ipser: J. Phase Equilib. Diffus., **37** (2016) 459.
[22] D. An, S. Zhang, X. Zhai, W. Yang, R. Wu, H. Zhang, W. Fan, W. Wang, S. Chen, O. Cojocaru-Miredin, X. Zhang, M. Wuttig, and Yu: Nat. Commun., **15** (2024) 3177.
[23] X. Zhang, Z. Bu, X. Shi, Z. Chen, S. Lin, B. Shan, M. Wood, A. H. Snyder, L. Chen, G. J. Snyder, and Y. Pei: Sci. Adv., **6** (2020) eabc0726.
[24] M. T. Ange, P. W. Voorhees, and G. J. Snyder: Adv. Mater., **31** (2019) 1902980.
[25] J. Zheng and W. Davenport: Phys. Rev. B., **69** (2004) 144415.
[26] G. Rahman, S. Cho, and S. C. Hong: J. Magn. Magn. Mater., **304** (2006) e146.
[27] H. Kim, Z. M. Gibbs, Y. Tang, H. Wang, and G. J. Snyder: APL Mater., **3** (2015) 041506.
[28] The Materials Project: MnSb (mp-786). (2023)
[29] The Materials Project: FeSb (mp-2619). (2023)